Applied Thermal Engineering 139 (2018) 562–568

Contents lists available at ScienceDirect

Applied Thermal Engineering

journal homepage: www.elsevier.com/locate/apthermeng

Research Paper

Performance comparison of jet pumps with round and sharp edge of small opening in oscillatory flow

Ye Feng[a], Ke Tang[a,b,c,*], Tao Jin[a,b], Kaihao Zhang[c], Rui Yang[a]

[a] College of Energy Engineering, Zhejiang University, 38 Zheda Road, Hangzhou 310027, China
[b] Key Laboratory of Refrigeration and Cryogenic Technology of Zhejiang Province, Zhejiang University, 38 Zheda Road, Hangzhou 310027, China
[c] Department of Mechanical Science and Engineering, University of Illinois, 1206 West Green Street, Urbana, IL 61801, USA

HIGHLIGHTS

- Effect of rounding on a jet pump is systematically investigated.
- Jet pump with sharp edge induces reversed and higher time-averaged pressure drop.
- A jet pump with rounding at small opening can work more efficiently.
- The optimal taper angles for sharp and round edge jet pumps are different.

ARTICLE INFO

Keywords:
Thermoacoustic engine
Jet pump
Oscillatory flow
Time-averaged pressure drop

ABSTRACT

Owing to the capability to induce a time-averaged pressure drop in oscillatory flow, a jet pump has been used to suppress the Gedeon streaming in a looped thermoacoustic engine. The suppression capacity originates from the asymmetric pressure drop through the jet pump, and could be enhanced by rounding the edge of the jet pump in traditional view. This paper systematically probes the rounding effect on a jet pump and compares the performance of jet pumps with round and with sharp edge on small opening. The performance dependences on the taper angle and the cross-sectional area ratios, including the big-to-small opening area ratio of the jet pump and the small opening-to-pipe cross sectional area ratio, are analyzed and compared for the two types of jet pump. The results reveal a reversed and higher time-averaged pressure drop in the shape edge jet pump in contrast to that in the rounded jet pump. However, the round edge of the small opening can improve working efficiency of a jet pump.

1. Introduction

A traveling-wave thermoacoustic engine, due to its inherently reversible thermodynamic cycle [1], is an attractive solution for converting thermal energy into acoustic power. In 1999, Backhaus and Swift successfully developed a typical traveling-wave thermoacoustic engine [2], which achieved a thermal efficiency as high as 0.3, and boosted up the development and applications in such extensive fields as electrical power generation [3–5], refrigeration [6–8] and water pumping [9], etc. Despite the higher theoretical efficiency in a traveling-wave thermoacoustic system, an acoustic streaming named as Gedeon streaming [10] may occur in the closed-loop configuration of the traveling-wave thermoacoustic engine, and has a detrimental influence on the system thermal efficiency [2,11–14].

To suppress the Gedeon streaming, a jet pump was frequently used in the looped configuration [2,12,13,15]. The jet pump is a tapered hole with different opening areas. The pressure drop through the jet pump is asymmetric in two opposite directions along the channel axis during the two half time periods, which can result in a time-averaged pressure drop in oscillatory flow. An appropriate time-averaged pressure drop can be used to suppress the Gedeon streaming. So far, the time-averaged pressure drop is usually calculated by the formula proposed by Backhaus and Swift [2,13], which is based on the quasi-static hypothesis [16]:

$$\Delta p_a = \frac{\rho U_{1,jp}^2}{8a_s^2}\left\{\left[k_{exp,s} + \left(\frac{a_s}{a_b}\right)^2 k_{con,b}\right] - \left[\left(\frac{a_s}{a_b}\right)^2 k_{exp,b} + k_{con,s}\right]\right\}, \quad (1)$$

where ρ is the mean density of working fluid, a indicates the area of the jet pump. $U_{1,jp}$ is the volumetric velocity amplitude through the jet pump. k_{exp} and k_{con} are the loss coefficients for expansion and

* Corresponding author at: College of Energy Engineering, Zhejiang University, 38 Zheda Road, Hangzhou 310027, China.
E-mail address: ktang@zju.edu.cn (K. Tang).

https://doi.org/10.1016/j.applthermaleng.2018.05.023
Received 16 November 2017; Received in revised form 22 February 2018; Accepted 7 May 2018
Available online 08 May 2018
1359-4311/

contraction. The subscripts s and b denote the small and the big opening of the jet pump, respectively.

It is routinely accepted that edge rounding on the small opening of a jet pump can strengthen the asymmetric pressure drop induced by the jet pump in the oscillatory flow [2]. Due to the decrease of $k_{con,s}$ in Eq. (1), the round edge of the small opening can reduce the pressure drop in the diverging direction [17], then increase the time-averaged pressure drop in the converging direction. With this result, there are intensive studies on the jet pump with round edge (JP-R) [18–21], however, the performance of the jet pump with sharp edge (JP-S) is rarely discussed.

Notably, our previous numerical simulation has shown that the flow separation may exist in the diverging direction of a jet pump, especially for JP-S [22], leading to a significant effect on the time-averaged pressure drop. Furthermore, preliminary experimental results reveal that the time-averaged pressure drop induced by JP-S is opposite to that induced by JP-R [23]. In additional, the direction of time-averaged pressure drop induced by JP-S opposites with that calculated by Eq. (1). This indicates that the Eq. (1) could wrongly predict the direction of time-averaged pressure drop Δp_a induced by JP-S. Such a jet pump designed based on Eq. (1) might not prevent Gedeon streaming and even promote it along with engine efficiency degradation. Biwa et al.'s [12] experimental results also presented that installing the jet pump with wrong orientation, the heat loss was increased from 6.5 W to 30 W, when the input heat power supplied to the prime mover was 100 W.

However, just one JP-S structure has been tested in our previous experiment. It is not yet clear the opposite time-averaged pressure drop phenomenon is ubiquitous in JP-S, and the performance of JP-S with different configurations is still unknown. Therefore, it is of great significance to generalize the rounding effects on a jet pump and rationalize a generic design strategy.

In this work, the time-averaged pressure drop induced by JP-S and its dependences on the taper angle and the big-to-small opening area ratio of the jet pump are investigated experimentally. A deal of attention is put on the performance comparison of JP-S and JP-R studied in our previous research [23]. Subsequently, the influence of small opening-to-pipe cross sectional area ratio on the time-averaged pressure drop induced by jet pump is further analyzed.

2. Experimental system

2.1. Experimental apparatus

The experimental setup consists of a linear compressor, a tested jet pump, a particle packing chamber and a reservoir, as shown schematically in Fig. 1. The detailed description can be found in our previous work [23]. The pressure-wave generator is a linear compressor of type CP6231. The linear motor has a dual-opposed configuration with two same motors to eliminate the vibration and increase the output. The linear motor has a displacement limitation of 6 mm. The swept volume is $2.3 \times 10^{-5}\,m^3$, and the backside chamber volume of one motor is $2.3 \times 10^{-3}\,m^3$. The dead volume between the two pistons, i.e., the space volume in front of the pistons is $1.3 \times 10^{-4}\,m^3$. The tested jet pump is a component with a tapered hole, as shown in Fig. 2. The dimensions are listed in Table 1. Nos. 1–16 are parameters for JP-S, and Nos. 17–22 are for JP-R. The dimensionless rounding at the edge of the small opening r/d_s is 0.3, where r is the rounding radius and d_s is the diameter of the smallest cross section. All the deviations of diameters and lengths are within ± 0.05 mm, and those of taper angles are ± 0.1°. At researching the taper angle influence, the cross-sectional areas a_b and a_s are fixed, and α depends on the length of jet pump L_{jp}. Meanwhile, the effects of two cross-sectional area ratios, i.e., the ratio of the big-to-small opening of jet pump a_b/a_s and the ratio of the small opening-to-pipe cross sectional area a_s/A are analyzed.

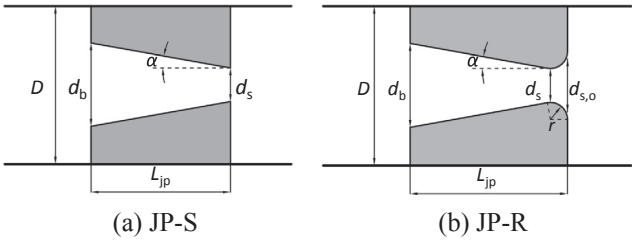

Fig. 2. Schematic of the jet pumps.

For the oscillating flow, a resistance-and-compliance (RC) load, usually used for measuring the acoustic power output from thermoacoustic engines [2,24], is adopted to characterize the velocity through the jet pump. The RC load often takes the form of a needle valve combined with a reservoir. However, the opening of the needle valve is sufficiently small, which may affect the flow field inside the pipe substantially. Here, instead of the needle valve, a particle packing chamber filled with particle filler is used to provide resistance in our experimental apparatus. The volume of reservoir V_{res} is 1 L. The diameter of the pipe D is 28 mm. The performance of the jet pump is tested at 60 Hz with nitrogen as the working gas at a pressure of 3 MPa.

2.2. Measurement

The measured parameters include six pressures and three temperatures, as shown in Fig. 1. Two piezoelectric pressure sensors P1 and P2 (PCB PIEZOTRONICS 113B28), which are located at two sides away from the jet pump at the same distance of 6D, are used to measure the dynamic pressure on each side of the jet pump, with accuracies of 3.447 kPa. A two-way differential UNIK-5000-type pressure sensor P3, with the range of −200 to 200 kPa and the accuracy of 0.2% FS, is used to measure the differential pressure across the jet pump. The mean pressures measurement employ two UNIK-5000-type pressure sensors P4 and P5, with the ranges of 0–5 MPa and the accuracy of 0.2% FS. Since the pressure amplitude in the reservoir is the key parameter for calculating the velocity amplitude and much smaller, a piezoelectric pressure sensor P6 (PCB PIEZOTRONICS 106B) with an accuracy of 0.57 kPa is used for more accurate measurement of the dynamic pressure in the reservoir. Three sheathed platinum resistance thermometers (PT100) (i.e., T1, T2 and T3), are used to measure the temperatures of

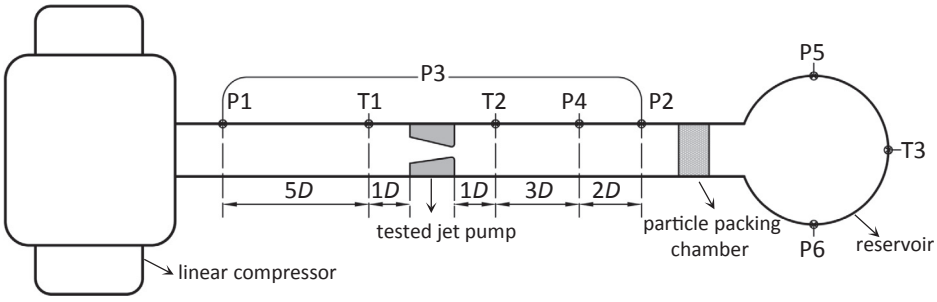

Fig. 1. Schematic of the experimental apparatus (Labeled P or T indicate the pressure or temperature are measured, D = 28 mm).

Table 1
Dimensions of the jet pump.

No.	α (°)	d_s (mm)	d_b (mm)	L_{jp} (mm)	No.	α (°)	d_s (mm)	d_b (mm)	L_{jp} (mm)
1	5	7	10	17.2	12	15	5	10.3	10
2	7	7	10	12.2	13	15	6	12.4	12
3	9	7	10	9.5	14	15	8	16.6	16
4	12	7	10	7.1	15	15	9	18.6	18
5	15	7	10	5.6	16	15	10	20.7	20
6	20	7	10	4.1	17	9	5	7.6	9.8
7	15	7	11.3	8	18	9	6	9.1	11.7
8	15	7	12.2	9.7	19	9	7	10.6	13.7
9	15	7	13.5	12.1	20	9	8	12.1	15.7
10	15	7	14.5	14	21	9	9	13.6	17.6
11	15	7	16	16.8	22	9	10	15.1	19.6

working gas at each end of the jet pump and in the reservoir, with accuracies of ± 0.1 °C.

3. Data reduction

For the data reduction, it is assumed that the resistance coefficient of the fluid through the jet pump in one direction is constant, and the velocity is assumed to be sinusoidal. Therefore, the time-averaged pressure drop and acoustic power loss can be written as [2,23]:

$$\begin{aligned}\Delta p_a &= \int_0^T \Delta p(t)\mathrm{d}t/T \\ &= \rho u_1^2\left(\int_0^{T/2}\tfrac{1}{2}k_+\sin^2\omega t\mathrm{d}t-\int_{T/2}^{T}\tfrac{1}{2}k_-\sin^2\omega t\mathrm{d}t\right)\Big/ T=\tfrac{1}{8}\rho u_1^2(k_+-k_-),\end{aligned} \tag{2}$$

$$\begin{aligned}\Delta E_a &= \int_0^T \Delta p(t)U_{1,jp}(t)\mathrm{d}t/T \\ &= a_s\rho u_1^3\left(\int_0^{T/2}\tfrac{1}{2}k_+\sin^3\omega t\mathrm{d}t-\int_{T/2}^{T}\tfrac{1}{2}k_-\sin^3\omega t\mathrm{d}t\right)\Big/ T=\tfrac{a_s}{3\pi}\rho u_1^3(k_+ + k_-)\end{aligned} \tag{3}$$

where T is the time period, u_1 is the velocity amplitude through the small opening of jet pump, and ω is the angular frequency. k represents the resistance coefficient. The subscripts + and − represent in the forward flow and the backward flow, i.e., the flow in the converging direction and the diverging direction, respectively.

The time-averaged pressure drop Δp_a is measured by P3. The acoustic power loss ΔE_a can be calculated by

$$\Delta E_a = \frac{1}{2}\mathrm{Re}(p_{1,1}\widetilde{U}_{1,1})-\frac{1}{2}\mathrm{Re}(p_{1,2}\widetilde{U}_{1,2}) \tag{4}$$

where $p_{1,1}$ and $p_{1,2}$ are the pressure amplitudes measured by P1 and P2. $U_{1,1}$ and $U_{1,2}$ are the volumetric velocity amplitudes on each side of the jet pump, respectively. Diacritical mark ~ stands for complex conjugate.

Based on the analogy of acoustics and electrics [2], the velocity amplitude through the small opening of jet pump u_1 in Eqs. (2) and (3) can be calculated by

$$\begin{aligned}u_1 &= \frac{U_{1,jp}}{a_s} = \rho_{res}\frac{i\omega C_{res}p_{1,res} + i\omega C_2 p_{1,2}}{\rho_{jp}a_s} \\ &= \rho_{res}\frac{i\omega V_{res}p_{1,res}/p_{m,res} + i\omega V_2 p_{1,2}/p_{m,pi}}{\gamma\rho_{jp}a_s},\end{aligned} \tag{5}$$

where C_{res} and C_2 denote acoustic compliances of the reservoir and the pipe between the reservoir and the jet pump, respectively. $p_{1,res}$ and $p_{1,2}$ are the pressure amplitudes in the reservoir and pipe behind the jet pump, which are measured by P6 and P2, respectively. V_2 is the volume of the pipe between the reservoir and jet pump. $p_{m,res}$ and $p_{m,pi}$ are the mean operating pressures in the reservoir and pipe, which are measured by P5 and P4, respectively. γ is the specific heat capacity ratio of the working fluid. ρ_{res} and ρ_{jp} are the densities of fluid in the reservoir and jet pump, respectively. Meanwhile, the volumetric velocity amplitudes in each side of the jet pump $U_{1,1}$ and $U_{1,2}$ can be calculated by

$$U_{1,1} = U_{1,jp}-\rho_{res}\frac{i\omega C_1 p_{1,1}}{\rho_{jp}} = \frac{i\omega V_{res}p_{1,res}\rho_{res}}{\gamma\rho_{jp}p_{m,res}} + i\omega\rho_{res}\frac{V_2 p_{1,2}-V_1 p_{1,1}}{\gamma\rho_{jp}p_{m,pi}}, \tag{6}$$

$$U_{1,2} = \rho_{res}\frac{U_{1,res}-i\omega C_3 p_{1,2}}{\rho_{jp}} = \frac{i\omega V_{res}\rho_{res}p_{1,res}}{\gamma\rho_{jp}p_{m,res}}-\frac{i\omega\rho_{res}V_3 p_{1,2}}{\gamma\rho_{jp}p_{m,pi}}, \tag{7}$$

where C_1 and V_1 are the acoustic compliance and the volume of connecting pipe between P1 and jet pump, respectively. C_3 and V_3 denote the acoustic compliance and the volume of connecting pipe between P2 and reservoir, respectively.

A desire jet pump in a thermoacoustic engine should provide a sufficient time-averaged pressure drop Δp_a with a smaller acoustic power loss ΔE_a for suppressing Gedeon streaming efficiently. Therefore, we pay more attention to the two evaluating parameters, i.e., time-averaged resistance k_a, and the coefficient of effectiveness ε, which have been proposed in our previous study [22]. The definitions are as follows

$$k_a = \frac{\Delta p_a}{\int_0^T\frac{\rho u^2}{2}\mathrm{d}t} = \frac{\int_0^{T/2}\frac{\rho u^2}{2}k_+\mathrm{d}t-\int_{T/2}^{T}\frac{\rho u^2}{2}k_-\mathrm{d}t}{\frac{1}{4}\rho u_1^2} = \frac{k_+-k_-}{2} = \frac{4\Delta p_a}{\rho u_1^2}, \tag{8}$$

$$\varepsilon = \left|\frac{\Delta p_a}{\Delta E_a}\right|. \tag{9}$$

Obviously, k_a represents to the capability of a jet pump to produce the time-averaged pressure drop. And a higher ε implies that a jet pump can work more efficiently. Subsequently, k_a and ε are used to compare the performance of JP-S and JP-R in this study. Meanwhile, according to Eqs. (2) and (3), k_+ and k_- can be calculated.

Reynolds number in an oscillatory flow can be defined as [19]:

$$Re = \frac{u_1\delta_\nu\rho}{\mu}, \tag{10}$$

where μ is the dynamic viscosity of the working fluid. δ_ν is the viscous penetration depth, $\delta_\nu = (2\upsilon/\omega)^{1/2}$, which is approximately 53 μm. υ is the kinematic viscosity of the working fluid. In order to identify the fluid flow status, the critical Reynolds number Re_c given by Ohmi and Iguchi is used here to determine the transformation from laminar to turbulent flow [25]:

$$Re_c = 305\left(\frac{d_s}{\delta_\nu}\right)^{1/7}. \tag{11}$$

The critical Reynolds numbers Re_c for different d_s are shown in Table 2. In this work, Re is always larger than Re_c, indicating that these

Table 2
Critical Reynolds number Re_c.

d_s (mm)	5	6	7	8	9	10
Re_c	584	599	613	625	635	645

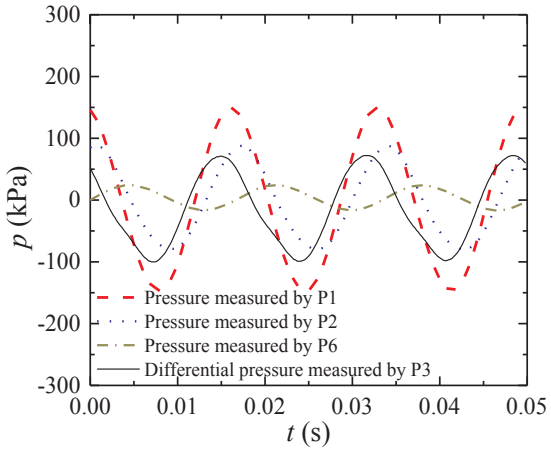

Fig. 3. Function of pressures with time.

measurements are in the turbulent regime. The numerical simulation of jet pump in the turbulent oscillatory flow is so intricate that there are inadequate explorations about jet pump behavior in this regime. Therefore, measurements in the turbulent regime deserve more attention.

4. Experimental results of jet pump performance

The measurement of the pressure is of great importance to calculate the two evaluating parameters k_a, and ε as shown in Eqs. (8) and (9). Therefore, before comparing the performances in detail, we firstly present the functions of temporal acoustic pressures with time for No. 3 jet pump in Table 1 operating at $Re = 6 \times 10^3$. As shown in Fig. 3, the dynamic pressures at two sides of the jet pump and in the reservoir measured by pressure sensors P1, P2 and P6 as well as the differential pressure across the jet pump measured by pressure sensor P3 are almost sinusoidal waveform.

4.1. Impact of taper angle α

Firstly, we discuss the effect of taper angle α on performance of JP-S, and compare the results with the performance of a JP-R in our previous study [23]. In this part, the cross-sectional areas a_b and a_s are fixed, and α depends on the length of jet pump L_{jp}. To clearly elucidate the taper angle effect, we keep the same a_b and a_s in both JP-S and JP-R for comparison. The dependences of k_+ and k_- with α are depicted in Fig. 4. For the forward flow, k_+ of JP-S (Nos. 1–6 in Table 1) and JP-R seem insensitive to α, while JP-R has a smaller k_+ than JP-S. This may be due to the expansion loss decreases in JP-R as the channel outlet $a_{s,o}$ increases after rounding. In the backward flow, k_- of JP-S is obviously lager than that of JP-R, and the variations of k_- with a rise in α between the two types of jet pump are different. That is, k_- of JP-S significant increases with a rise in α when α is less than 12°, while k_- of JP-R changes very slightly with a smaller α, and increases slowly as α increases beyond 9°. In the backward flow, i.e., in the diverging direction, due to the restraint at the sharp entrance contracts the flow, the flow seperates from the wall severely [22]. This will lead to the cross-sectional area of channel is much larger than the actual flowing area, which causes the velocity of the main flow at the exit is much larger than the theoretical value $a_s u_1/a_b$. The expansion loss at the exit in the diverging direction can be calculated by $\Delta p_{exp} = \frac{1}{2}\rho k_{exp} u^2$, where $k_{exp} = (1 - a/A)^2$. Therefore, the increase of velocity of the main flow eventually leads to the increase in the expansion loss. Meanwhile, with the increase of α, the velocity of main flow further increases at the exit, implying the flow separation become more serious, which results in the rise of k_-. However, the onset of flow separation has been delayed until α is larger than 9° after rounding due to the large curvature between the small opening and the tapered surface of the jet pump, as presented in Fig. 4(b). Notably, the decrease in k_- after rounding can be attributed to the reduce of flow seperation, which results in the notable decrease in the expansion loss at the outlet a_b in the backward flow, but not the decrease in $k_{con,s}$.

Fig. 5 shows the dependence of k_a and ε on α. As presented in Fig. 5(a), JP-S has a negative k_a, indicating that the time-averaged pressure drop is in the diverging direction, which is different from the case in JP-R. When α is 5°, k_a for JP-R is slightly larger than the absolute value of negative k_a for JP-S. However, as α increases beyond 5°, JP-S has a higher potential to produce the time-averaged pressure drop than JP-R, especially for the jet pump with a larger α, indicated by the larger absolute value of k_a for JP-S than that for JP-R. Moreover, the maximum absolute value of k_a for JP-S is obviously larger than that for JP-R, and the directions are opposite. In this case, the traditional understanding that edge rounding of small opening increases the time-average pressure drop becomes worrisome, since the influence of flow separation on k_- is not considered. On the other hand, it should be noted that since the direction of the time-averaged pressure drop for JP-S is in the diverging direction, the development of flow separation dose not deteriorate the jet pump performance as it is traditionally believed to, but improves the time-averaged pressure drop.

As for working efficiency, Fig. 5(b) shows the different variations of ε for JP-S and JP-R with a rise in α. Within the small α regime, JP-R shows the higher ε than that in JP-S, however, JP-S becomes more efficient when α is larger than 12°. In contrast to the previous studies [23], this gives JP-S a chance to work more efficiently than JP-R under

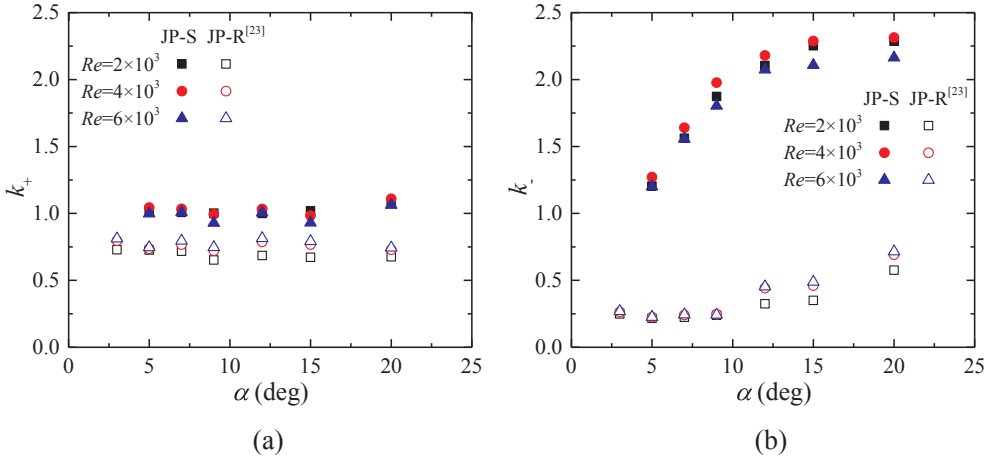

Fig. 4. Variations of coefficients of resistance k_+ (a) and k_- (b) with α.

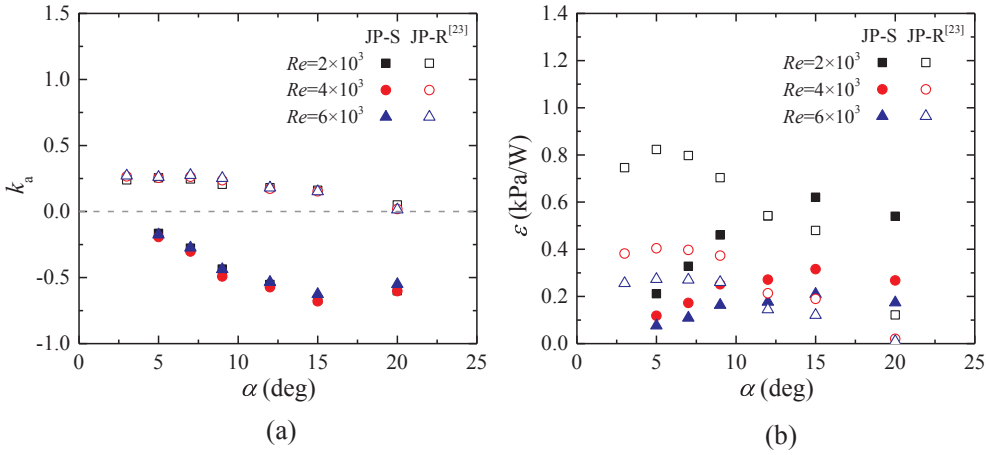

Fig. 5. Variations of coefficient of time-averaged resistance k_a (a) and coefficient of effectiveness ε (b) with α.

the same *Re* in high α regime. And decreasing *Re* can increase the working efficiency for both JP-S and JP-R.

4.2. Impact of cross-sectional area ratio a_b/a_s

The influence of a_b/a_s is discussed in the following section. As mentioned before, JP-S with α larger than 12° can induce a larger time-averaged pressure drop efficiently, while for JP-R, it has a relatively higher performance with α in the range of 3–9°, and exhibits instant performance deterioration as α increases beyond 9°. To gain a better performance comparison between JP-S and JP-R, the comparative analysis of the impact of a_b/a_s is based on the optimized α. To be specific, the taper angle α is 15° (Nos. 5, 7–11 in Table 1) in JP-S, and the performance is compared with that of JP-R with α of 9° [23]. Due to the larger optimal α in JP-S, the length of jet pump L_{jp} is only 5.6 mm when a_b/a_s is 2 (the corresponding ratio of length to diameter L_{jp}/d_s is 0.8), thus the jet pump with a_b/a_s less than 2 is not considered here.

The variations of k_+ and k_- with a_b/a_s are shown in Fig. 6. For JP-R, k_+ is insensitive to a_b/a_s, but k_- decreases with the increase of a_b/a_s, due to the decrease of expansion loss in the backward flow [23]. JP-S shows the different behavior, k_+ and k_- exhibit negligible fluctuations as a_b/a_s increases, which implies that the change of a_b/a_s has little effect on the flow separation. The variations of k_a and ε with a_b/a_s are depicted in Fig. 7. JP-S has a noticeably larger absolute value of k_a than JP-R. However, when a_b/a_s is larger than 2, JP-R can work more efficiently than JP-S. For the jet pump with a fixed α, the length of jet pump L_{jp} depends on a_b/a_s. As for JP-S, the variance of k_a with a_b/a_s is small, similar variance of ε can be observed in Fig. 7(b), which indicates that the change of a_b/a_s has little effect on the performance of JP-S with α of 15°. Therefore, the length of JP-S can be reduced to make the engine more compact. However, for the case of JP-R, the time-averaged pressure drop and the working efficiency can be improved by increasing a_b/a_s when a_b/a_s is less than 2.3. As a result, the required length for JP-R has to be long to maintain the high performance, since the optimal ε is reached when a_b/a_s is larger and α is smaller.

4.3. Impact of cross-sectional area ratio a_s/A

The above analyses are carried out on the jet pumps with the same small opening area a_s. To be more systematic, the effect of the ratio of the small opening-to-pipe cross sectional area a_s/A on the jet pump performance is studied. The aforementioned α and a_b/a_s show the different influences on the performance of JP-S and JP-R. Therefore, in the following discussion, we keep the two types of jet pump at the optimal performance even though the α and a_b/a_s are different. For JP-R, α is 9°, and a_b/a_s is 2.3 (Nos. 17–22 in Table 1). JP-S has α of 15° and a_b/a_s of 4.3 (Nos. 10, 12–16 in Table 1), and its length is closed to that of JP-R under the same a_s/A. We have investigated the dependences of k_+ and k_- on a_s/A. As presented in Fig. 8, it is noted that both JP-R and JP-S have negative change in k_+ and k_- with a rise in a_s/A, which implies that under a given velocity amplitude u_1 through the small opening, the pressure drops along the channel axis during the two half time periods for jet pumps with different a_s/A are comparatively closed.

The variations of k_a and ε with a_s/A are depicted in Fig. 9. JP-R and

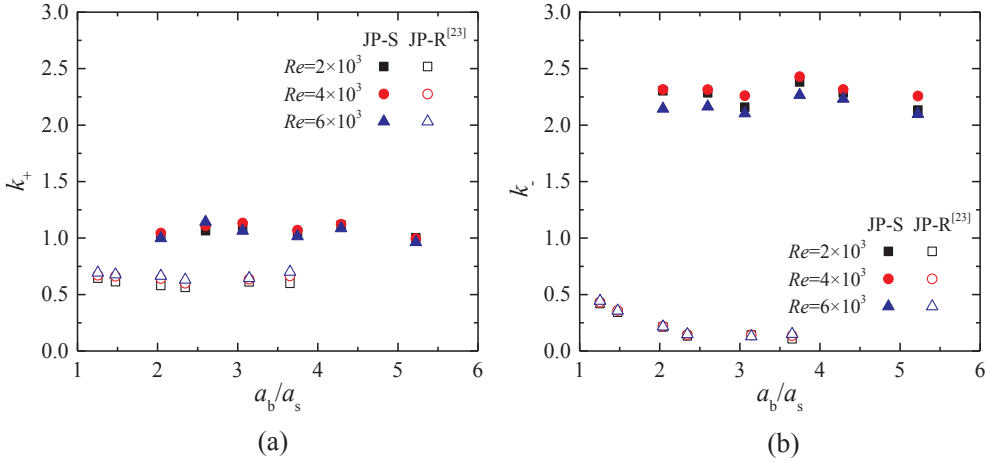

Fig. 6. Variations of coefficients of resistance k_+ (a) and k_- (b) with a_b/a_s.

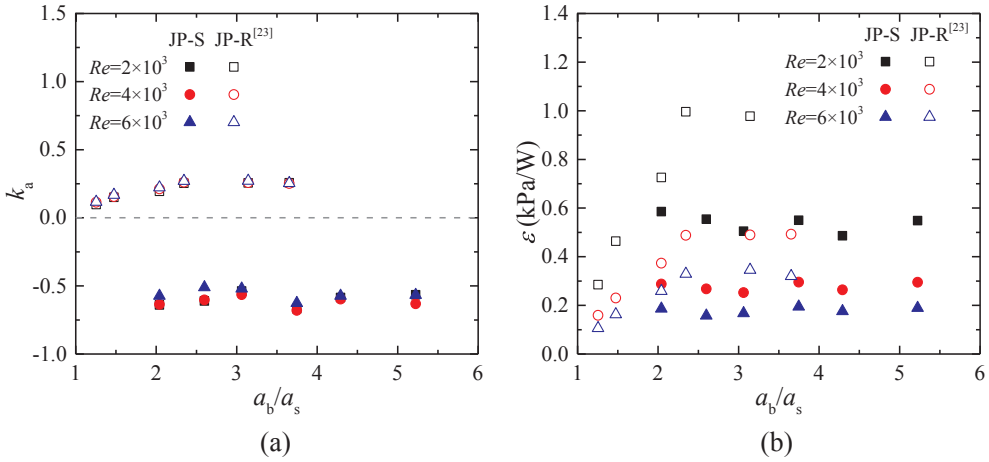

Fig. 7. Variations of coefficient of time-averaged resistance k_a (a) and coefficient of effectiveness ε (b) with a_b/a_s.

JP-S show significant dependence of ε on a_s/A, while their k_a seem to be insensitive to a_s/A. As for ε, it increases with the decrease of a_s/A. To be specific, for a given u_1, the time-averaged pressure drops induced by the jet pumps with different a_s/A are almost constant, which can be verified by the small change of k_a. On the other hand, the volumetric velocity amplitude through the jet pump reduces with the decrease of a_s/A and results in a smaller acoustic power loss, as shown in Eq. (3). This leads to the increase of working efficiency with the decrease of a_s/A.

5. Conclusion

This paper focuses on the performance comparison between the jet pump with sharp edge (JP-S) and the jet pump with round edge (JP-R). The performance dependences on the configurations including the taper angle α and the cross-sectional area ratios (a_b/a_s and a_s/A) are analyzed. The experimental results and the corresponding analyses elucidate the edge rounding effect on the performance of a jet pump in the looped thermoacoustic system:

(1) The direction of the time-averaged pressure drop induced by JP-S is in the diverging direction, which is opposite to that induced by JP-R. This can be attributed to the intensive flow separation in JP-S, which boosts up the pressure drop in the diverging direction and even larger than that in the converging direction. Notably, the development of flow separation in JP-S dose not deteriorate the jet pump coefficient of effectiveness, but enhances the time-averaged pressure drop.

(2) The optimized α and a_b/a_s between JP-S and JP-R are different. For JP-S, increasing α is conducive to the high time-averaged pressure drop and working efficiency when α is less than 15°. Meanwhile, the change of a_b/a_s has little effect on the performance of JP-S, indicating that the length of jet pump can be reduced to make the engine more compact. However, in order to guarantee the high performance in JP-R, the jet pump with α less than 9° and relatively larger a_b/a_s is recommended [23]. Additionally, when a_s/A is in the range of 0.03–0.13, the change of a_s/A has little effect on coefficient of time-averaged resistance k_a, but reducing a_s/A can significantly increase the working efficiency of both JP-S and JP-R.

(3) Comparison of the optimal results of JP-S and JP-R shows that the absolute value of k_a for JP-S is obviously larger than that for JP-R, and JP-S exhibits a higher ε than JP-R in high α cases. Our analyses imply that a JP-S can be more promising to induce the time-averaged pressure drop and thus suppress the Gedeon streaming. Therefore, the traditional understanding that edge rounding of small opening is beneficial to increase the time-averaged pressure drop could be ambiguous. However, applying JP-R could improve the working efficiency, due to the significant decrease of pressure drop in the diverging direction.

In addition, it is noted that a structure with a reduced cross-sectional area has the capability to change the phase relation between the pressure and the velocity oscillation, which will also affect the efficiency of the thermoacoustic engine [26–28]. Therefore, both the time-averaged pressure drop and the phase-change effect need to be

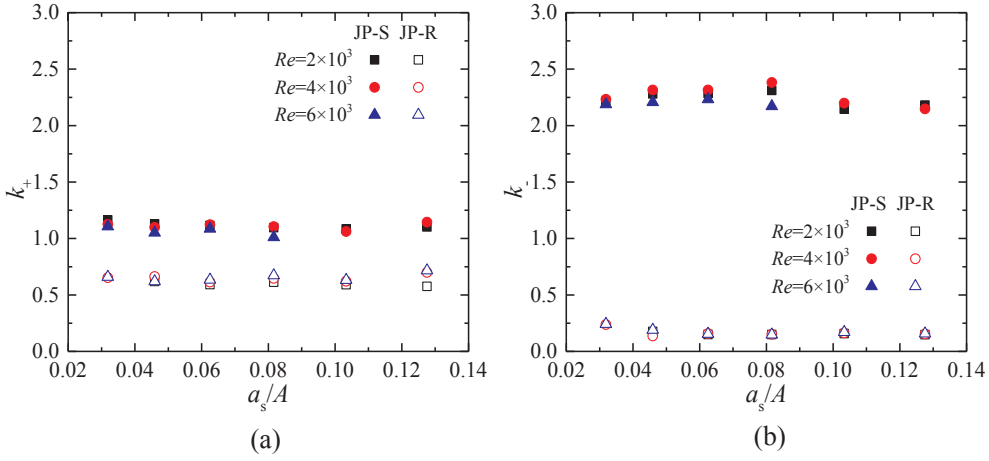

Fig. 8. Variations of coefficients of resistance k_+ (a) and k_- (b) with a_s/A.

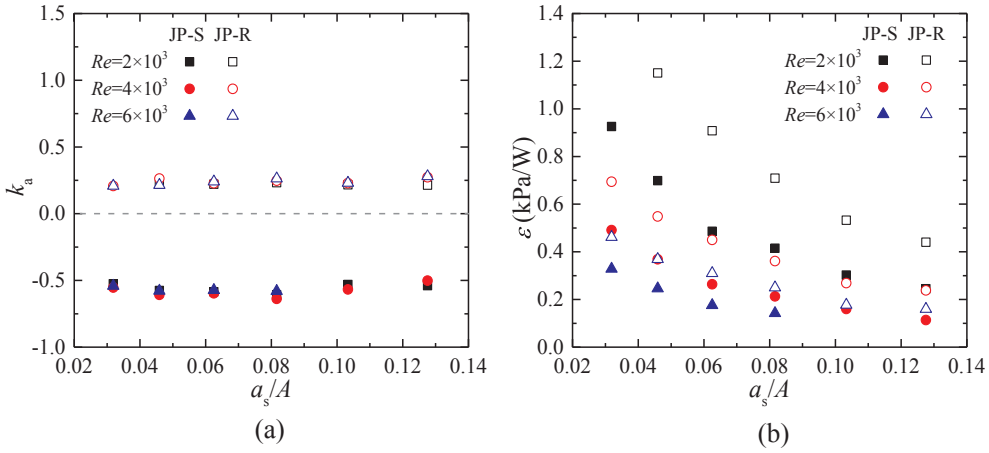

Fig. 9. Variations of coefficient of time-averaged resistance k_a (a) and coefficient of effectiveness ε (b) with a_s/A.

considered for the design of the jet pump. Compared to JP-R, the variation in the length of JP-S has little influence on its performance of inducing time-averaged pressure drop, which gives more room to the phase-chance optimization during the jet pump design.

Acknowledgements

This work is financially supported by the National Natural Science Foundation of China (Grant Nos. 51376158 and 51576170) and the National Key Research and Development Program of China (Grant No. 2016YFB0901403).

Appendix A. Supplementary material

Supplementary data associated with this article can be found, in the online version, at http://dx.doi.org/10.1016/j.applthermaleng.2018.05.023.

References

[1] P.H. Ceperley, A pistonless Stirling engine—the traveling wave heat engine, J. Acoust. Soc. Am. 66 (5) (1979) 1508–1513.
[2] S. Backhaus, G.W. Swift, A thermoacoustic-Stirling heat engine: detailed study, J. Acoust. Soc. Am. 107 (6) (2000) 3148–3166.
[3] Z.B. Yu, A.J. Jaworski, S. Backhaus, Travelling-wave thermoacoustic electricity generator using an ultra-compliant alternator for utilization of low-grade thermal energy, Appl. Energy 99 (2012) 135–145.
[4] T.J. Bi, Z.H. Wu, L.M. Zhang, G.Y. Yu, E.C. Luo, W. Dai, Development of a 5 kW traveling-wave thermoacoustic electric generator, Appl. Energy 185 (2017) 1355–1361.
[5] T. Jin, R. Yang, Y. Wang, Y. Feng, K. Tang, Low temperature difference thermoacoustic prime mover with asymmetric multi-stage loop configuration, Sci. Rep. 7 (1) (2017) 7665.
[6] R. Bao, G.B. Chen, K. Tang, W.H. Cao, T. Jin, Thermoacoustically driven pulse tube refrigeration below 80K by introducing an acoustic pressure amplifier, Appl. Phys. Lett. 89 (2006) 211915.
[7] S. Hasegawa, T. Yamaguchi, Y. Oshinoya, A thermoacoustic refrigerator driven by a low temperature-differential, high-efficiency multistage thermoacoustic engine, Appl. Therm. Eng. 58 (1–2) (2013) 394–399.
[8] L.M. Zhang, J.Y. Hu, Z.H. Wu, E.C. Luo, J.Y. Xu, T.J. Bi, A 1 kW-class multi-stage heat-driven thermoacoustic cryocooler system operating at liquefied natural gas temperature range, Appl. Phys. Lett. 107 (3) (2015) 033905.
[9] C.N. Markides, A. Gupta, Experimental investigation of a thermally powered central heating circulator: pumping characteristics, Appl. Energy 110 (2013) 132–146.
[10] D. Gedeon, DC gas flows in Stirling and pulse tube cryocoolers, in: R.G. Ross (Ed.), Cryocoolers 9, Plenum Press, New York, 1997, pp. 385–392.
[11] G.Y. Yu, E.C. Luo, W. Dai, J.Y. Hu, Study of nonlinear processes of a large experimental thermoacoustic-Stirling heat engine by using computational fluid dynamics, J. Appl. Phys. 102 (7) (2007) 074901.
[12] T. Biwa, Y. Tashiro, M. Ishigaki, Y. Ueda, T. Yazaki, Measurements of acoustic streaming in a looped-tube thermoacoustic engine with a jet pump, J. Appl. Phys. 101 (6) (2007) 064914.
[13] P. Yang, Y.W. Liu, G.Y. Zhong, Prediction and parametric analysis of acoustic streaming in a thermoacoustic Stirling heat engine with a jet pump using response surface methodology, Appl. Therm. Eng. 103 (2016) 1004–1013.
[14] K. Tang, Y. Feng, T. Jin, S.H. Jin, M. Li, R. Yang, Effect of Gedeon streaming on thermal efficiency of a travelling-wave thermoacoustic engine, Appl. Therm. Eng. 115 (2017) 1089–1100.
[15] S. Boluriaan, P.J. Morris, Suppression of traveling wave streaming using a jet pump, 41st AIAA Aerospace Sciences Meeting and Exhibit, AIAA, Reno, NV, 2003, pp. 1–11.
[16] M. Iguchi, M. Ohmi, K. Meagawa, Analysis of free oscillatory flow in a U-shaped tube, Bull. JSME 25 (1982) 1398–1405.
[17] I.E. Idelchik, Handbook of Hydraulic Resistance, third ed., Begell House, New York, 1996.
[18] A. Petculescu, L.A. Wilen, Oscillatory flow in jet pumps: nonlinear effects and minor losses, J. Acoust. Soc. Am. 113 (3) (2003) 1282–1292.
[19] B.L. Smith, G.W. Swift, Power dissipation and time-averaged pressure in oscillatory flow through a sudden area change, J. Acoust. Soc. Am. 113 (5) (2003) 2455–2463.
[20] J.P. Oosterhuis, S. Bühler, T.H. van der Meer, D. Wilcox, A numerical investigation on the vortex formation and flow separation of the oscillatory flow in jet pumps, J. Acoust. Soc. Am. 137 (4) (2015) 1722.
[21] M.A. Timmer, J.P. Oosterhuis, S. Bühler, D. Wilcox, T.H. van der Meer, Characterization and reduction of flow separation in jet pumps for laminar oscillatory flows, J. Acoust. Soc. Am. 139 (2016) 193–203.
[22] K. Tang, Y. Feng, S.H. Jin, T. Jin, M. Li, Performance comparison of jet pumps with rectangular and circular tapered channels for a loop-structured traveling-wave thermoacoustic engine, Appl. Energy 148 (2015) 305–313.
[23] Y. Feng, K. Tang, T. Jin, K.H. Zhang, R. Yang, Time-averaged pressure drop induced by a jet pump in oscillatory flow, J. Acoust. Soc. Am. 142 (2017) 1730–1738.
[24] K. Tang, Z.J. Huang, T. Jin, G.B. Chen, Influence of acoustic pressure amplifier dimensions on the performance of a standing-wave thermoacoustic system, Appl. Therm. Eng. 29 (2009) 950–956.
[25] M. Ohmi, M. Iguchi, Critical Reynolds number in an oscillating pipe flow, Trans. Jpn. Soc. Mech. Eng. B 25 (1982) 165–172.
[26] T. Biwa, Y. Ueda, T. Yazaki, U. Mizutani, Work flow measurements in a thermoacoustic engine, Cryogenics 41 (2001) 305–310.
[27] Y.W. Liu, P. Yang, Influence of inner diameter and position of phase adjuster on the performance of the thermoacoustic Stirling engine, Appl. Therm. Eng. 73 (2014) 1141–1150.
[28] T. Jin, R. Yang, Y. Wang, Y.L. Liu, Y. Feng, Phase adjustment analysis and performance of a looped thermoacoustic prime mover with compliance/resistance tube, Appl. Energy 183 (2016) 290–298.